Fast Single-Mode Fiber Nonlinearity Monitoring: An Experimental Comparison Between Split-Step and Nonlinear Fourier Transform-Based Methods

Pascal de Koster, Olaf Schulz, Jonas Koch, Stephan Pachnicke, *Senior Member, IEEE*, and Sander Wahls, *Senior Member, IEEE*

***Abstract*—We experimentally investigate the problem of monitoring the Kerr-nonlinearity coefficient γ from transmitted and received data for a single-mode fiber link of 1600 km length. We compare the accuracy and speed of three different approaches. First, a standard split-step Fourier method is used to predict the output at various γ values, which are then compared to the measured output. Second, a recently proposed nonlinear Fourier transform (NFT)-based method, which matches solitonic eigenvalues in the transmitted and received signals for various γ values. Third, a novel fast version of the NFT-based method, which only matches the highest few eigenvalues. Although the NFT-based methods do not scale with link length, we demonstrate that the SSFM-based method is significantly faster than the basic NFT-based method for the considered link of 1600 km, and outperforms even the faster version. However, for a simulated link of 8000 km, the fast NFT-based method is shown to be faster than the SSMF-based method, although at the cost of a small loss in accuracy.**

***Index Terms*—Single-mode fiber, Kerr-nonlinearity, characterization, split-step Fourier method, nonlinear Schrödinger equation, nonlinear Fourier transform, forward scattering transform, solitons.**

I. Introduction

THE characterization of the Kerr nonlinearity coefficient of an installed optical fiber link is fundamental for fiber optical communications when employing higher launch powers, for example for digital back-propagation (DBP) [1], [2], [3], [4], nonlinear frequency division multiplexing (NFDM) [5], or for performance estimation [6]. However, the nonlinearity coefficient is often not well known by the operator, so it is critical to measure the nonlinearity coefficient to optimally choose the transmission system parameters afterwards. Even when estimates of the nonlinearity coefficients are provided by the manufacturer, the coefficients may vary slightly between fibers, or change after installation due to aging, bending or splicing [1]. The re-characterization or even continuous monitoring of installed fibers is therefore often beneficial or even necessary. Monitoring of the nonlinearity coefficient can furthermore reveal changes of the link.

Practical communication systems today often avoid high powers at which the Kerr-nonlinear effect starts to distort the signal significantly. Therefore, the exact value of the Kerr-nonlinearity coefficient received little attention so far. However, as optical networks are being pushed towards higher bit-rates - often employing higher launch powers - estimating the Kerr-nonlinearity coefficient becomes increasingly important. We are thus interested in methods to accurately and quickly determine the value of the Kerr-nonlinearity coefficient. Many links are in constant use. Furthermore, the transmission format is often difficult to change. Hence, it would be desirable to use already available regular transmission data to identify the Kerr-nonlinearity coefficient. This implies that the usual identification methods relying on specific training signals (e.g., using four-wave mixing [7], cross-phase modulation [8] or self-phase modulation [9]) are not well-suited for characterization of operational links. Instead, the Kerr-nonlinearity coefficient is typically identified by numerically simulating the propagation through the link with a split-step Fourier method (SSFM), for various nonlinearity coefficients. The nonlinearity coefficient at which the numerically forward-propagated input matches the measured output best is kept [10], [11], [12], [13]. However, the time required by such methods increases with the fiber length. They are therefore more time consuming for long links.

In earlier work, we proposed an alternative identification method which does not directly depend on the link length. This method compares solitonic components found using the nonlinear Fourier transform (NFT) of the transmitted and received signals [14], [15]. Solitons are stable waves that arise from a balance between dispersive and nonlinear effects. In an idealized lossless and noise-free link, the eigenvalues associated with the solitons are conserved exactly during propagation. Nevertheless, even in the presence of loss and noise the solitonic eigenvalues are still very stable [1]. As hidden solitons are present in many kinds of typical fiber-optical transmission data [15], [16], the

Manuscript received 4 September 2023; revised 29 September 2023; accepted 2 October 2023. Date of publication 9 October 2023; date of current version 20 October 2023. *(Corresponding author: Pascal de Koster.)*

Pascal de Koster is with the Delft Center for System and Control (DCSC), Delft University of Technology, 2628 CD Delft, The Netherlands (e-mail: p.b.j.dekoster@tudelft.nl).

Olaf Schulz and Stephan Pachnicke are with the Chair of Communications, Kiel University, 24143 Kiel, Germany (e-mail: olaf.schulz@tf.uni-kiel.de; stephan.pachnicke@tf.uni-kiel.de).

Jonas Koch was with the Chair of Communications, Kiel University, 24143 Kiel, Germany. He is now with Rohde & Schwarz GmbH & Co KG, 24118 Kiel, Germany.

Sander Wahls was with Delft Center for System and Control, TU Delft, 2628CD Delft, The Netherlands. He is now with the Institute of Industrial Information Technology, Karlsruhe Institute of Technology, 76187 Karlsruhe, Germany (e-mail: sander.wahls@kit.edu).

Digital Object Identifier 10.1109/JPHOT.2023.3322635

NFT-based identification method is in principle widely applicable. The Kerr-nonlinearity coefficient is required to normalize the data before computing the NFT, and thus affects the detected solitons. The NFT-based identification method compares the solitonic components at the transmitter and receiver for different values of the Kerr-nonlinearity coefficient, and keeps the one at which the solitonic components match best. No numerical propagation is necessary. Thus the method does not depend on the link length, in contrast to propagation based-methods. We thus investigate if a speed-up can be achieved with respect to SSFM-based methods by instead comparing the signals in the NFT domain.

The NFT-based method has been investigated in simulations [14] and experiments [15], [17], where it has been found to provide similar estimates to split-step methods. However, it has not yet been tuned and assessed in terms of computational complexity, which is the goal of this article. We propose and investigate a faster version of the NFT-based nonlinearity characterization from [15], which only considers a few high-energy solitons. (While all nonlinear Fourier components are required to reconstruct a signal, one component in general is already sufficient to estimate the fiber parameters under ideal circumstances.) The solitonic eigenvalues are computed faster by using the old eigenvalues at an earlier γ estimate as initial guesses for the eigenvalues at the new γ estimate. This drastically speeds up the NFT-based matching, at the cost of some accuracy.

Finally, we quantitatively compare the SSFM-based identification method, the NFT-based method from [15] and the faster NFT-based method in terms of speed and accuracy. We first compare these three methods on well-separated pulses, such that neighboring pulses do not distort each other due to channel memory. Next, we compare the three methods on signal segments, that have been cut out from a full burst. As the channel memory distorts the received signal segment, we adapt the SSFM-based method slightly to take this into account. The NFT-based methods were less affected by the distortion due to channel memory and were therefore not adjusted.

The main contributions in this article are thus as follows:

- **The proposal of a novel fast version of the NFT-based nonlinearity identification algorithm.**
- **An experimental investigation of the accuracy of the SSFM-based method, the original NFT-based method and the novel NFT-based method.**
- **A run-time comparison of these three algorithms.**

This article is organized as follows. Section II describes the nonlinearity identification algorithm through the split-step Fourier method. Section III recapitulates how the NFT can be used to identify solitonic components in a signal, and to identify the nonlinearity coefficient. Section IV describes the proposed faster NFT-based method which only compares the highest few eigenvalues. Section V compares the three identification methods on experimental measurement data for a 1600 km link. Section VI compares the three identification methods on simulated data for an 8000 km link. Finally, Section VII concludes the article.

II. Split-Step Fourier Method for Fiber Nonlinearity Identification

The propagation of an optical signal through a span of single-mode fiber (SMF) can be modeled by the lossy nonlinear Schrödinger equation (NLSE),

$$A_l = -i\frac{\beta_2}{2}A_{\tau\tau} + i\gamma|A|^2A - \frac{\alpha}{2}A, \tag{1}$$

in which A (in $\sqrt{\mathrm{W}}$) is the complex signal amplitude, l (in m) the distance, τ (in s) the time, β_2 (in $\frac{\mathrm{s}^2}{\mathrm{m}}$) the second-order dispersion coefficient, α (in $\frac{1}{\mathrm{m}}$) the loss coefficient, and finally γ (in $\frac{1}{\mathrm{Wm}}$) the Kerr-nonlinearity coefficient to be identified in this article. Subscripts denote partial derivatives. At the end of each span an Erbium-doped fiber amplifier (EDFA) boosts the signal to a fixed launch power, resulting in a sawtooth-like power profile over the entire link.

In the first method considered in this article, the nonlinear coefficient γ is determined by numerically propagating the transmitted signal for various γ values, and keeping the γ value at which the forward propagated input and measured output match best. Here, we use the split-step Fourier method (SSFM) for the digital propagation. This method simulates the evolution of an optical signal by propagating the signal numerically in spatial steps of size Δl [18]. Each step is split up in a linear part and a nonlinear part. The linear part solves the effects of the linear terms in the NLSE analytically in the Fourier domain. Let $\tilde{A}(\omega, l) = \mathcal{F}\{A(\tau, l)\}$ be the Fourier transform of A, then the linear part of the NLSE is solved in the Fourier domain through

$$\tilde{A}^{\mathrm{lin}}(\omega, l+\Delta l) = \tilde{A}(\omega, l)\, e^{\left(i\frac{\beta_2}{2}\omega^2 - \frac{\alpha}{2}\right)\Delta l}. \tag{2}$$

Next, the nonlinear contribution is added by assuming that $|A(\tau, l)|^2$ is approximately constant during the spatial step, and the contribution is again added in the Fourier domain:

$$\tilde{A}(\omega, l+\Delta l) = \tilde{A}^{\mathrm{lin}}(\omega, l+\Delta l)\, e^{i\gamma\mathcal{F}\{|A^{\mathrm{lin}}(\omega, l+\Delta l)|^2\}\Delta l}. \tag{3}$$

At the end of each fiber span, the signal is numerically amplified to model the EDFA loss compensation. However, no amplified spontaneous emission (ASE) noise is added in the simulation, since we consider an idealized propagation.

In order to determine the best value of γ, we consider the relative L_1-error between the measured output and the numerically propagated input:

$$E(\gamma) = \frac{\int_T \left(|A^{\mathrm{out}}(\tau) - A^{\mathrm{out,SSFM}}(\tau;\gamma)|\right)\,\mathrm{d}\tau}{\int_T |A^{\mathrm{out}}(\tau)|\,\mathrm{d}\tau}, \tag{4}$$

in which $A^{\mathrm{out}}(\tau)$ is the measured received signal, $A^{\mathrm{out,SSFM}}(\tau;\gamma)$ the transmitted signal after numerical propagation with γ, and $T = [T_0,\ T_1]$ the time window of the considered signal. This error is evaluated for every γ in a grid, and the γ with the smallest error is kept. For the numerical propagation, the transmitted signal is first re-sampled using Fourier interpolation at sampling frequency equal to four times the 99%-energy bandwidth of the transmitted signal. We found that this sampling rate was required to obtain accurate results.

We note here that the identified γ implicitly depends on the assumed values of β_2 and α using the SSFM-method (this will also hold for the NFT-based methods). Using wrong values here implies that the value of γ does not correspond to the actual value of the fiber. However, the identified value will still correspond to the γ describing the system best given the assumed α and β, and would therefore still be 'optimal' for the purpose of signal processing.

The spatial step Δl is chosen as large as possible, but small enough that the identified value for γ has converged. The propagation part of the SSFM-based method is performed using a fast *C* version of the software *ssprop* [19], while the error is calculated in *MATLAB*. This SSFM-based method requires $\mathcal{O}(N\log(N)L)$ floating point operations (FLOPs), where L is the total link length, and $N\log(N)$ is the computational cost of the fast Fourier transforms.

A. SSFM-Based Identification From Windowed Signals

The SSFM-based algorithm processes a burst of a finite duration. The boundaries of the burst should contain sufficient guard intervals in order to account for signal broadening and the periodicity of the discrete Fourier transform. When only a cut-out part of the burst is processed, the guard intervals are missing and these effects have to be taken into account.

We formally define a 'windowed' signal as a segment (i.e., window) $q(\tau)$, $\tau \in [T_0, T_1]$, cut-out from a full signal. The windowed signal is identical to the full signal for the duration of the window. The numerical SSFM propagation implicitly assumes that outside the window, the signal repeats periodically, and thus the numerical propagation will differ from the physical propagation. However, this difference is only limited to a boundary region at the edges of the window. We approximate the size of the affected boundary region using the formula for pulse broadening (pb) [1, Eq. 2.3.3]:

$$\Delta T^{\text{pb}} = |L\beta_2\Delta\Omega|, \tag{5}$$

where ΔT^{pb} is the amount that a Gaussian-shaped signal with radial bandwidth $\Delta\Omega$ gets broader as it travels through a fiber of length L with dispersion coefficient β_2. For the purpose in this article, it sufficed to estimate the pulse broadening using only the dispersion, as we noticed that the contribution of nonlinearity to pulse broadening was insignificant in comparison to the dispersion for the considered links.

We found that we only need to cut away a quarter of the pulse broadening at both window boundaries to sufficiently prevent the influence of the pulse broadening. We can thus define an interior region of the window, that is barely affected by the windowing of the signal. We define the interior of the window as

$$T^{\text{int}} = \left[T^{\text{int}}_{\text{left}}, T^{\text{int}}_{\text{right}}\right] = \left[T_0 + \tfrac{1}{4}\Delta T^{\text{pb}},\, T_1 - \tfrac{1}{4}\Delta T^{\text{pb}}\right]. \tag{6}$$

When the SSFM-based method is applied to windowed signals, we will simulate the propagation of the windowed signal in the whole window T, but only consider the error on the interior T^{int}:

$$E(\gamma) = \frac{\int_{T^{\text{int}}} \left(|A^{\text{out}}(\tau) - A^{\text{in, SSFM}}(\tau;\gamma)|\right)\, \mathrm{d}\tau}{\int_{T^{\text{int}}} |A^{\text{out}}(\tau)|\, \mathrm{d}\tau}. \tag{7}$$

III. Nonlinear Fourier Transform-Based Fiber Nonlinearity Identification Using Solitons

An alternative method for fiber-nonlinearity identification considers the solitonic content in transmitted signals. Solitons are stable, particle-like waves resulting from a balance between the dispersive and the nonlinear effects. Due to their stability, solitons existing in the transmitted signal are normally also present at the receiver, while only moderately affected by noise. Although solitons are often not directly recognizable from the signal shape, earlier research has already shown that many conventional fiber-optic transmission signals contain significant amounts of solitons [14], [16], [20]. The nonlinear Fourier transform (NFT) can be used to determine the solitonic spectrum of a signal, in which the nonlinearity coefficient γ plays the role of a parameter that is used to normalize the signal. When the correct γ value is assumed in the normalization, the solitons at the transmitter are identical to the solitons at the receiver for a noiseless and lossless fiber, while a wrong γ value will result in a mismatch between transmitted and received solitons. We may thus identify γ by determining the value at which the transmitted solitons and received solitons match best. The greatest advantage of NFT-based identification is that no signal propagation is required. The required time of the method therefore does not directly scale with the link length, as opposed to the SSFM-based method. In the following, we recapitulate the most important aspects of NFT-based nonlinearity identification.

A. Normalized Nonlinear Schrödinger Equation

The soliton content of a signal may be determined using the nonlinear Fourier transform. The NFT is typically computed from the lossless normalized and dimensionless NLSE. To obtain a lossless NLSE, we apply path-averaging to the lossy NLSE from 1:

$$Q = Ae^{\alpha l/2}, \quad \gamma_1 = \frac{1}{L_{\text{s}}}\int_0^{L_{\text{s}}} \gamma e^{-\alpha l}\, \mathrm{d}l = \gamma\frac{1-e^{-\alpha L_{\text{s}}}}{\alpha L_{\text{s}}}, \tag{8}$$

$$\Rightarrow Q_l \approx -i\frac{\beta_2}{2}Q_{\tau\tau} + i\gamma_1|Q|^2Q, \tag{9}$$

where γ_1 is the path-averaged nonlinearity coefficient, and L_{s} is the uniform span-length. Finally, the equation is normalized [21]:

$$t = \frac{1}{T_0}\tau, \quad q = T_0\underbrace{\sqrt{|\gamma_1/\beta_2|}}_{c_q}Q, \quad z = \frac{1}{T_0^2}\underbrace{(-\beta_2/2)}_{c_z}l, \tag{10}$$

$$\Rightarrow q_z = iq_{tt} + 2i|q|^2q, \tag{11}$$

where c_q is the amplitude normalization constant (c_q^2 is the effective nonlinearity-dispersion ratio of the fiber link), and c_z the space normalization constant. The time normalization $T_0 \neq 0$ is a free parameter. Similar to the linear Fourier transform, it simply re-scales the NFT spectrum. Throughout this article, we use the receiver sampling time $T_0 = \Delta t = 0.0125\,\text{ns} = 1/(80\,\text{GHz})$.

B. Nonlinear Fourier Transform

After normalizing the signal according to the fiber parameters β_2, γ, α, and L_s, the solitons can be extracted by computing the NFT of $q(t)$. The NFT is found by solving the Zakharov-Shabat scattering problem [22],

$$\frac{\mathrm{d}}{\mathrm{d}t}\begin{bmatrix}\phi_1(t,\lambda)\\ \phi_2(t,\lambda)\end{bmatrix} = \begin{bmatrix}-i\lambda & q(t)\\ -q^*(t) & i\lambda\end{bmatrix}\begin{bmatrix}\phi_1(t,\lambda)\\ \phi_2(t,\lambda)\end{bmatrix}, \tag{12a}$$

$$\text{s.t.}\begin{bmatrix}e^{-i\lambda t}\\ 0\end{bmatrix} \overset{t\to-\infty}{\longleftarrow} \begin{bmatrix}\phi_1(t,\lambda)\\ \phi_2(t,\lambda)\end{bmatrix} \overset{t\to+\infty}{\longrightarrow} \begin{bmatrix}a(\lambda)e^{-i\lambda t}\\ b(\lambda)e^{+i\lambda t}\end{bmatrix}, \tag{12b}$$

in which $\phi(t,\lambda)$ is the eigenfunction corresponding to the complex spectral parameter $\lambda = \xi + i\eta$, and $a(\lambda)$ and $b(\lambda)$ are the scattering coefficients indicated by the right boundary conditions in 12b. The full NFT spectrum finally consists of a discrete (solitonic) spectrum, and a continuous spectrum. We define the continuous spectrum as the value of $b(\lambda)$ over the real axis, $\Lambda^{\mathrm{c}} := \{b(\xi) : \xi \in \mathbb{R}\}$, and the discrete spectrum using the zeros of $a(\lambda)$ in the upper half plane, $\Lambda^{\mathrm{d}} := \{(\lambda_k, b(\lambda_k)) : \Im(\lambda_k) > 0, a(\lambda_k) = 0\}$. Each eigenvalue $\lambda_k = \xi_k + i\eta_k$ corresponds to a soliton. The eigenvalue λ_k defines the shape and speed of the soliton, while the b-coefficient $b_k = b(\lambda_k)$ provides information about the soliton location and phase [23]. Throughout the rest of this article, we are only interested in the eigenvalues.

C. Nonlinearity Identification From Eigenvalue Matching

The Kerr-nonlinearity coefficient may be determined by comparing the NFT spectra of a transmitted signal and its corresponding received signal for various values of γ, which influence the NFT spectra through the normalization in 8–11. As the value of γ is varied, there is an optimal value at which the NFT spectra at the transmitter and the receiver match best. While both the continuous spectrum and discrete spectrum may be used for spectral matching, the continuous spectrum often contains little power. We observed that the power in the continuous spectrum of the considered signals was only 2% at 2 dBm, 6% at -1 dBm, 10% at -4 dBm and 15% at -7 dBm signal power. The power in the continuous spectrum thus seems to be low, which, for some NFT-based transmitters, can even be proven mathematically [24]. In general many signals close to the linear regime still have a significant portion of their energy in the discrete spectrum, and can contain many solitons [14], [16]. There are also specifically designed nonlinear frequency division multiplexed (NFDM) signals that only use the continuous spectrum [25]. In such situations, the discrete spectrum version of the algorithm from [14] cannot be utilized, but instead the version for the continuous spectrum given there should be used. Finally, it was also observed in [14] that using the continuous spectrum of low-energy signals to determine γ also causes significant bias. We therefore chose not to use the continuous spectrum for identification.

We thus only consider the discrete spectrum, and follow the discrete spectrum matching method used in [14] and [15], which is summarized below:

1) A γ value is selected from a grid, and its corresponding c_q value is used for the normalization.
2) The eigenvalues of the transmitted and received signals are determined from the normalized signals.
3) The matching error E is determined as follows:

$$E = \min_{m(k)} \frac{\sum_k E_{km(k)}}{\sum_k \Im\left(\lambda_k^{\mathrm{in}}\right) + \sum_m \Im\left(\lambda_m^{\mathrm{out}}\right)}, \quad \text{with} \tag{13a}$$

$$E_{km} = \min\left(|\lambda_m^{\mathrm{out}} - \lambda_k^{\mathrm{in}}|, \Im(\lambda_k^{\mathrm{in}} + \lambda_m^{\mathrm{out}})\right), \tag{13b}$$

where $m(k)$ denotes the perfect matching which connects the input eigenvalue λ_k^{in} to the output eigenvalue λ_m^{out}, and E_{km} is the cost of connecting these eigenvalues. In case the input and output spectra have different numbers of eigenvalues, unmatched eigenvalues of the larger spectrum are assigned a maximum cost: $E_{k-} = \Im(\lambda_k^{\mathrm{in}})$, $E_{-m} = \Im(\lambda_m^{\mathrm{out}})$. By assigning a maximum cost to eigenvalue pairs and to unmatched eigenvalues, each eigenvalue cannot contribute more to the error than its associated energy ($\propto \Im\lambda_k$). This ensures that random low eigenvalues with very little energy do not dominate the error, but the high (energetic) eigenvalues are most important. After assigning each matching a cost, the minimum-cost matching may be efficiently determined (e.g., using the Hungarian algorithm [26]).

The steps 1)–3) are repeated for every γ value in the grid. The γ value with the lowest error is kept. This procedure is performed for each signal block, and all estimates for γ are averaged for a final estimate.

For this method, we found accurate results when using a sampling rate of two times the bandwidth of the transmitted signal, so only half the number of samples compared to the SSFM-based method. The full discrete spectrum was determined using the software library *FNFT* (branch *add_bsloc_methods2*, commit 9756b3) [27]. We used the default sub-sample and refine method with the *4split4B* discretization. The desired number of samples after sub-sampling was chosen using the Nyquist rate. In this configuration finding the eigenvalues requires $\mathcal{O}(N^2)$ FLOPs, where N is the number of samples.

D. NFT-Based Identification From Windowed Signals

When considering a windowed signal, the NFT implicitly assumes it to be zero outside the window while in reality it is not. The unaccounted interactions with the outside lead to distortions in the soliton spectra. We investigated the option of deriving the location of each soliton based on its b-coefficient, and only accept the eigenvalues that were inside the interior for the matching. However, we found that doing so did not significantly improve the NFT-based identification. We therefore decided to omit it.

We investigated why accepting and discarding solitons based on their location did not significantly improve the identification algorithm. We found that windowing mostly influences the low eigenvalues, but their contribution to the full error is very limited. Furthermore, we observed that most of the medium and high eigenvalues appear inside the interior by default, and also stay

there during propagation. We believe there are two reasons for this.

First, any potentially high eigenvalue close to the edge has part of its soliton cut off, and its eigenvalue is thus lowered in the process. Most of the detected high eigenvalues are thus already inside the interior. Second, all large solitons (corresponding to high eigenvalues) have a short duration, and thus large bandwidth. This large bandwidth should fit entirely within the signal bandwidth, and thus their center frequency lies closer to the center (i.e., zero). The drift speed of each soliton is proportional its center frequency [21], which is therefore also relatively low. The highest solitons therefore have relatively low drift speeds, and thus usually stay within the window during the transmission.

As accepting and rejecting eigenvalues due to the windowing does not seem to influence the highest eigenvalues too much, we will use the same NFT-based algorithm for both full signals and windowed signals.

IV. Fast NFT-Based Nonlinearity Identification Through Local Refinement of High Eigenvalues

In this section, we adapt the NFT-based algorithm from the previous section to speed it up, and create a fast NFT-based algorithm. To do so, we only consider the highest few eigenvalues of the signal. The highest eigenvalues contain most of the signal energy, and are also more robust to noise and model mismatch compared to lower eigenvalues. As we consider less information from the signal, the accuracy of the identified γ could slightly worsen. However, this loss in accuracy should be limited. It may even be beneficial to disregard the lower eigenvalues when they are known to be unreliable, as we will observe in some of the results.

The eigenvalues are a continuous function of γ. Therefore, as we sweep the value for γ in small steps, the eigenvalues at the new γ value will be close to the previous eigenvalues. We may thus refine the eigenvalues at the previous γ value to find the eigenvalues at the current γ value. Local refinement of the K highest eigenvalues only takes $\mathcal{O}(KN)$ FLOPs, as opposed to the $\mathcal{O}(N^2)$ FLOPs when the full spectrum has to be determined from scratch.

Our new strategy will be thus to compute a full spectrum only once, and then use the highest K eigenvalues as initialization for local refinement as the γ value is being varied. After the eigenvalues have been determined for the initial γ value, sweeping γ takes significantly less time than computing a full NFT at every γ.

The fast NFT-based identification algorithm proposed here is similar to the original NFT-based algorithm from Section III-C in the main lines. In both cases, we sweep over a grid of values for γ, and measure the error by how well the input- and output-eigenvalues match. The main difference is that we will now only match the highest few eigenvalues, and use a fast refinement method to update the eigenvalues when proceeding from one γ value to the next.

The full algorithm is summarized in Alg. 1, and has the following steps: 1)-2) Re-scale the time, the received signal and the transmitted signal using T_0. Normalize the transmitted and received signals using the $c_q(\gamma)$ (10) corresponding to the highest value of γ in the grid, resulting in normalized signals $q^{0,\text{in}}$ and $q^{0,\text{out}}$. 3)-4) Calculate the full discrete spectrum of $q^{0,\text{in}}$ and $q^{0,\text{out}}$ using the NFT in Section III-B. 5) Store the highest K^{high} input eigenvalues, and the highest 3 K^{high} output eigenvalues. These will be used as initial guesses. More output eigenvalues than input eigenvalues are kept, as we will only focus on matching all the highest input eigenvalues. When we took the same number of output eigenvalues as input eigenvalues, we found that the highest K input eigenvalues and highest K output eigenvalues found at the initial guess $c_q(1)$ would often not correspond to the highest K eigenvalues at the correct c_q as initially high eigenvalues often drift downwards as c_q is varied. To ensure that at the correct c_q all input eigenvalues have their correct counterpart present in the output eigenvalues, we thus need to consider more initial output eigenvalues than input eigenvalues. For the purpose in this article we observed that considering three times as many output eigenvalues usually sufficed to include the correct counterparts of all the considered input eigenvalues, while still keeping the computation time low by considering only a small set of eigenvalues. This step concludes the initialization of the input and output eigenvalues. 6) Loop over all values of $c_q(\gamma)$, starting with the highest value. Perform steps 7)–10) in every loop. 7) Normalize the transmitted and received signals corresponding to the current value $c_q(\gamma)$. 8)-9) Determine the K^{high} highest input eigenvalues, and the 3 K^{high} highest output eigenvalues, by locally refining (using Newton's method, *bsloc_newton* in *FNFT*) the eigenvalues found with previous normalization $c_q^{\text{j-1}}$. 10) From the current set of K^{high} input and 3 K^{high} output eigenvalues, calculate the matching

Algorithm 1: Identifying c_q by Matching High Eigenvalues.

Input:
- Transmitted signal, $A^{\text{in}}(\tau)$,
- Received signal, $A^{\text{out}}(\tau)$,
- Grid of decreasing normalization constants $c_q(1) > c_q(2) > \ldots > c_q(J)$,
- Number of high eigenvalues to compare, K^{high},
- Time normalization, T_0.

Output:
- c_q^{ID}.

Algorithm:
1: $t = \tau/T_0, \quad Q^{\text{in}}(t) = T_0\, A^{\text{in}}(\tau), \quad Q^{\text{out}}(t) = T_0\, A^{\text{out}}(\tau).$
2: $q^{0,\text{in}}(t) = c_q(1)Q^{\text{in}}(t), \quad q^{0,\text{out}}(t) = c_q(1)Q^{\text{out}}(t),$
3: $\{(\lambda_k^{0,\text{in}}, b_k^{0,\text{in}}), k = 1, \ldots, K^{\text{all}}\} \leftarrow \text{NFT}(q^{0,\text{in}}(t))$
4: $\{(\lambda_m^{0,\text{out}}, b_m^{0,\text{out}}), m = 1, \ldots, M^{\text{all}}\} \leftarrow \text{NFT}(q^{0,\text{out}}(t))$
5: Keep the highest K^{high} input eigenvalues, and highest 3 K^{high} output eigenvalues.
6: **for** $j = 1, \ldots, J$ **do**
7: $\quad q^{j,\text{in}}(t) = c_q(j)Q^{\text{out}}(t), \quad q^{j,\text{out}}(t) = c_q(j)Q^{\text{out}}(t)$
8: $\quad \{(\lambda_k^{j,\text{in}}, b_k^{j,\text{in}}), k \leq K^{\text{high}}\} \leftarrow \text{NFT}(q^{j,\text{in}}) \,\big|\, \lambda_k^{j-1,\text{in}}$
9: $\quad \{(\lambda_m^{j,\text{out}}, b_m^{j,\text{out}}), m \leq 3\,K^{\text{high}}\} \leftarrow \text{NFT}(q^{j,\text{out}}) \,\big|\, \lambda_m^{j-1,\text{out}}$
10: $E(j) \leftarrow (\{\lambda_k^{j,\text{in}}\}, \{\lambda_m^{j,\text{out}}\})$ from 14
11: Return $c_q(j)$, at which $E(j)$ is minimal.

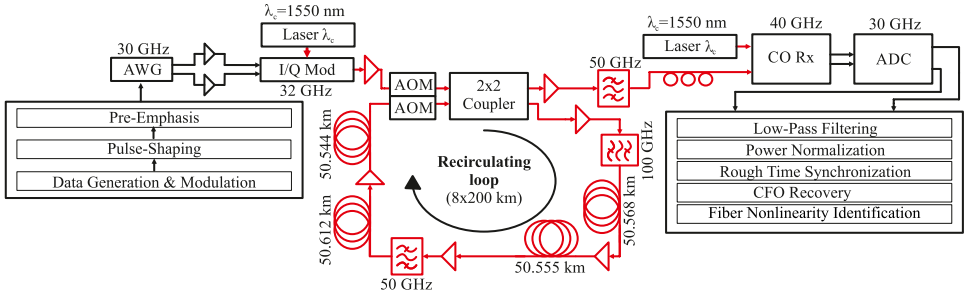

Fig. 1. Experimental setup with exact fiber lengths, positions of optical filters, and applied signal-processing. Acronyms: AWG = arbitrary waveform generator; AOM = acousto-optic modulator; CFO = carrier frequency offset.

error E as follows:

$$E = \frac{\sum_{k=1}^{K^{\text{high}}} E_{km(k)}}{\sum_{k=1}^{K^{\text{high}}} \Im\left(\lambda_k^{\text{in}}\right)}, \quad \text{with} \tag{14a}$$

$$E_{km} = \min\left(|\lambda_m^{\text{out}} - \lambda_k^{\text{in}}|, \Im(\lambda_k^{\text{in}})\right), \tag{14b}$$

where $m(k)$ is the minimum-cost matching [26], which assigns each input eigenvalue k to output eigenvalue m at the cost E_{km}. 11) After the error was determined for every c_q, return the value c_q at which the error is minimized. This concludes the algorithm.

We finally note that the same algorithm is used for full signals and for windowed signals, for the same reasons as in Section III-D.

V. Experimental Results

In this section, we compare the SSFM-based algorithm, the original NFT-based algorithm and the fast NFT-based algorithm with only high eigenvalues on experimental data. First, we compare the speed and accuracy of these three methods on full bursts separated by guard intervals. This ensures the signal is not influenced by neighboring pulses, which is implicitly assumed in both the SSFM-, and in the NFT-based methods. Second, we compare the three methods on windowed signals that are cut out from the same bursts. Windowing signals provides control over the signal length, and thus the computation time. However, this does imply that the edges of the windowed signals are affected by their surrounding, which is not the case for the complete bursts with guard intervals.

A. Experimental Setup

The experimental setup is shown in Fig. 1. All digital signals were pre-compensated for the measured frequency response of the back-to-back transceiver setup. Digital-to-analogue conversion was done using an 88 GSa/s arbitrary waveform generator (AWG). The analogue signal was converted into the optical domain at 1550 nm carrier wavelength using an I/Q modulator and a laser with <100 kHz linewidth. The optical signal was amplified to 2 dBm launch power before every fiber span, and circulated 8 times through a loop of 4 spans of 50 km OFS AllWave SMF for a total of 1600 km. Although higher launch powers are desirable for both nonlinear communication and identifying the nonlinearity coefficient, 2 dBm was the highest launch power we could use due to limitations in the experimental setup. The used launch power was well above the levels typically used in linear transmission, so the nonlinearity should still be sufficiently large to demonstrate and qualitatively compare all identification methods.

The reference fiber coefficients for α and β_2 were taken from the data sheet: $\beta_2^{\text{ref}} = -21.2\frac{\text{fs}^2}{\text{km}}(D = 16.6\frac{\text{ps}}{\text{nm·km}})$, $\alpha^{\text{ref}} = 0.19\frac{\text{dB}}{\text{km}}$. The value for γ was not provided by the data sheet, so we used a typical value from the literature [28, p.157] as initial guess: $\gamma^{\text{ref}} = 1.26\frac{1}{\text{Wkm}}$. After polarization de-rotation, the optical signal was received using a coherent receiver using a local laser with <10 kHz linewidth, and an oscilloscope with 80 GSa/s. The signal was post-processed as indicated in Fig. 1. Finally, we used the SSFM-based method with a space-step size of $\Delta l = 1000$ m, and the NFT-based methods to estimate the nonlinearity coefficient γ. Both the SSFM-based method and NFT-based methods were run on the same computer to ensure that the computation times shown in Table I can be fairly compared.

B. Identification From Complete Bursts

We first compare the identification algorithms on bursts with sufficient guard intervals, such that neighboring bursts do not interfere during the propagation. Therefore, the SSFM- and NFT-based methods can both be applied individually to each burst, without paying additional attention to interactions with neighboring bursts. Each burst consists of a summation of time-shifted raised cosine shaped carriers (roll-off factor 0.5), each multiplied with a symbol. More precisely, the transmitted signal $q^{\text{in}}(\tau)$ was given by

$$A^{\text{in}}(\tau) = \sum_{s}^{N_s} a_s A^{\text{c}}(\tau - sT^{\text{c}}), \quad \text{with} \tag{15a}$$

$$A^{\text{c}}(\tau) = \begin{cases} \frac{\pi}{4\,T^{\text{c}}}\text{sinc}\left(\frac{\tau}{T^{\text{c}}}\right), & \tau = \pm T^{\text{c}}, \\ \frac{1}{T}\text{sinc}\left(\frac{\tau}{T^{\text{c}}}\right)\frac{\cos(\pi\tau/2\,T^{\text{c}})}{1-(\tau/T^{\text{c}})^2)}, & \text{otherwise}, \end{cases} \tag{15b}$$

in which a_s is the QPSK-symbol with index s, $N_s = 128$ the number of symbols in a single burst, $T^{\text{c}} = 0.1$ ns the carrier spacing, and A^{c} the raised cosine carrier. The full burst duration with guard intervals was 16 ns. This signal-type was transmitted 100 times with random QPSK symbols over 1600 km at 2 dBm launch power. We observed that this type of signal contains

TABLE I
MEAN COMPUTATION TIME TO COMPUTE THE γ VALUE FROM A SINGLE BURST, FOR THE 6 DIFFERENT SIGNAL TYPES (DETAILS SPECIFIED PER ROW), USING THE FULL NFT-BASED METHOD, THE FAST NFT-BASED METHOD USING ONLY 10 EIGENVALUES, AND THE SSFM-BASED METHOD

Figure	# signal samples (×2 for SSFM)	# grid points for γ	bandwidth (99%)	launch power	amplification type	fiber length	comp. time per signal (NFT, full)	comp. time per signal (NFT, 10 EVs)	comp. time per signal (SSFM)	γ^{ID} [1/(W·km)] (NFT, full)	γ^{ID} [1/(W·km)] (NFT, 10 EVs)	γ^{ID} [1/(W·km)] (SSFM)
2	358	21	11 GHz	2 dBm	EDFA (50 km apart)	1600 km	13.0 s	2.53 s	2.40 s	1.20 ± 0.07	1.29 ± 0.10	1.20 ± 0.04
3a	72	21	11 GHz	2 dBm	EDFA (50 km apart)	1600 km	0.96 s	0.50 s	0.35 s	1.29 ± 0.13	1.30 ± 0.12	1.18 ± 0.12
3b	126	21	11 GHz	2 dBm	EDFA (50 km apart)	1600 km	2.32 s	1.15 s	0.48 s	1.31 ± 0.10	1.27 ± 0.09	1.18 ± 0.08
3c	180	21	11 GHz	2 dBm	EDFA (50 km apart)	1600 km	4.80 s	1.53 s	0.57 s	1.27 ± 0.10	1.25 ± 0.09	1.20 ± 0.06
6a	180	21	11 GHz	-4 dBm	EDFA (50 km apart)	1600 km	3.46 s	1.51 s	0.68 s	1.37 ± 0.20	1.31 ± 0.16	1.33 ± 0.18
6b	996	41	42 GHz	2 dBm	EDFA (50 km apart)	1600 km	725 s	8.45 s	6.30 s	1.59 ± 0.14	1.48 ± 0.22	1.28 ± 0.22
-	90	21	9 GHz	-3 dBm	ideal Raman	1600 km	0.81 s	0.54 s	0.56 s	1.20 ± 0.01	1.20 ± 0.02	1.20 ± 0.01
-	90	21	9 GHz	-3 dBm	ideal Raman	4800 km	0.69 s	0.31 s	1.79 s	1.20 ± 0.04	1.21 ± 0.04	1.20 ± 0.02
8a	90	21	9 GHz	-3 dBm	ideal Raman	8000 km	0.74 s	0.35 s	3.15 s	1.20 ± 0.03	1.20 ± 0.05	1.20 ± 0.03
-	536	21	11 GHz	-4 dBm	ideal Raman	1600 km	21.2 s	3.67 s	2.12 s	1.19 ± 0.03	1.21 ± 0.03	1.20 ± 0.01
-	536	21	11 GHz	-4 dBm	ideal Raman	4800 km	24.3 s	4.32 s	11.0 s	1.19 ± 0.03	1.22 ± 0.05	1.20 ± 0.01
8b	536	21	11 GHz	-4 dBm	ideal Raman	8000 km	21.42 s	4.11 s	19.05 s	1.20 ± 0.03	1.22 ± 0.05	1.20 ± 0.01
-	268	21	11 GHz	-4 dBm	ideal Raman	1600 km	10.4 s	2.23 s	1.93 s	1.20 ± 0.04	1.21 ± 0.04	1.20 ± 0.01
-	268	21	11 GHz	-4 dBm	ideal Raman	4800 km	10.0 s	2.03 s	5.72 s	1.20 ± 0.05	1.22 ± 0.06	1.20 ± 0.02
8c	268	21	11 GHz	-4 dBm	ideal Raman	8000 km	9.73 s	2.40 s	10.47 s	1.22 ± 0.06	1.23 ± 0.06	1.20 ± 0.03

For each signal type, the computation time for the identification was averaged over 100 bursts. The correct γ was 1.20 1/(W·km). The standard deviation in the distribution of the identified γ are also mentioned after the mean identified value.

about 70 solitons when normalized using $\gamma = 1.26\,1/(\mathrm{W{\cdot}km})$ (small variations occur depending due to the randomness of the symbols). The transmitted signals and corresponding received signals were used for the identification of γ. For a fair comparison, we consider the same grid of γ values for each of the three methods, and determine the error for every γ in the grid. The considered grid for the γ values ranged from $0.8\gamma^{\mathrm{ref}}$ to $1.2\gamma^{\mathrm{ref}}$, in 21 equidistant steps. We chose this grid as typical values of γ in data sheets include about 2% uncertainty [29]. A few percent difference in the used γ only marginally affect the received signal (and present solitons), and is typically acceptable for signal processing. The range of the grid was chosen large enough such that the distribution of estimated γ could be observed, as well as that we expect the correct γ to be within 20% of the reference value for the considered fiber.

For each of the methods, γ was identified for each of the 100 bursts, and a final estimate was calculated by averaging all estimates that were not at the edge of the grid. Estimates at the edge were discarded, as this implies that the error failed to converge within reasonable values for γ, and were thus considered outliers. The resulting γ distributions are shown in Fig. 2, and the final estimated γ values are shown in Table I.

We note that the distribution of the full NFT and SSFM-based methods are similar, and peak at approximately the same position of $\gamma = 1.20\,1/\mathrm{W{\cdot}km}$. We will consider this identified coefficient as the 'correct' coefficient to compare later results with. Although the full NFT-based method and SSFM-based method yield the same final estimate, the standard deviation of the distribution for the NFT-based method is larger than the variance for the SSFM-based method, which was also observed in an earlier study on simulation data [14]. We believe this is mostly due to the mismatch in the path-average approximation. In [30], it was shown that the stability of path-average second-order solitons in specific signals start to degrade significantly for signals around

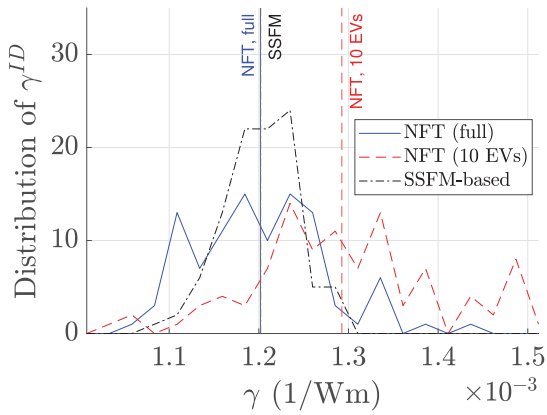

Fig. 2. Distribution of the identified γ from raised cosine bursts with vanishing tails.

2 dBm launch power, potentially explaining the large variance in the estimates for γ.

Next, we observe that the identified γ of the fast NFT-based method with 10 eigenvalues contains a 7% bias towards higher values of γ. We already observed that the input and output eigenvalues do not perfectly match due to the path-average approximation and noise, and that this causes a larger standard deviation for the identified γ. We suspect that the bias occurs because higher γ values generally create denser clouds of high eigenvalues, as more high eigenvalues are present due to more nonlinearity. The high input eigenvalues may then randomly find a closer output eigenvalue than at the correct γ, causing a bias towards slightly higher γ.

The computation times for the three identification algorithms are shown in Table I. We observe a speed-up of a factor 5 when considering only 10 eigenvalues in the fast NFT-based method compared to considering the full spectrum for every γ value.

The SSFM-based method was still slightly faster than the fast NFT-based method.

We thus conclude that the SSFM-based method resulted in the most accurately identified γ values, while also being the fastest method for this signal. However, with $N = 358$ samples, this signal was rather long. The original NFT-based method requires two full NFTs per γ value in the grid, so 42 NFTs in total for this grid. The fast NFT-based method also requires two full NFTs for initialization before the eigenvalue refinement. As both NFT-based methods calculate full NFTs, both require $\mathcal{O}(N^2)$ FLOPs, while the SSFM-based method only requires $\mathcal{O}(N \log N)$ FLOPs given that the number of spatial steps is kept constant. Considering shorter signals could thus allow NFT-based methods to perform faster. In the next section we therefore window the bursts to control the signal length, and compare the NFT- and SSFM-based methods on these signals.

C. Identification From Windowed Signals

In this section, we consider the identification of the nonlinearity coefficient from windowed signals (see Section II-A), short segments cut out from the bursts. In practical communication systems, bursts are often made as long as possible to minimize the impact of the guard interval on the spectral efficiency. Therefore, it will often occur that only long signals are available for the identification, so that windowing might significantly reduce the complexity. As opposed to the complete bursts from the previous subsection, the edges of the windowed signals will be affected by the signal outside the window, and thus this has an impact on the identification. On the other hand, windowing the signal has the benefit that the length of the considered signal can be controlled, and thus the identification may be sped up by considering shorter windows.

The SSFM-based method was slightly adapted to deal with the cut-off part of the bursts as described in Section II-A. For both NFT-based methods, we used the same algorithms as before, as explained in Section III-D.

For the identification in this section, we consider the raised cosine signals as in the previous section, but now consider only a small window centered around the middle of each raised cosine burst. A single block of the raised cosine signals had a duration of 16 ns, of which 3.2 ns was guard interval and the block of symbols was 12.8 ns. We are interested in the case where the considered window is a piece from a continuous stream of symbols, and thus we consider a center piece from the block which is sufficiently far away from the guard intervals. The pulse broadening (5) was approximately 1.2 ns. The smallest window we could theoretically consider would be 1.2 ns, but this entire window would then be influenced by the outside of the window. To ensure that we have a sufficiently large interior of the window, we chose the smallest window size as 3.2 ns.

The largest possible window size was 11.6 ns. Considering larger windows also becomes less efficient due to the superlinear scaling of the computation time as a function of signal duration. Instead of considering a long signal, it would be much faster to consider two signals with half the duration at some point. We thus chose the largest window to be 8.0 ns.

We also considered an intermediate window size of 5.6 ns. For these three different window sizes, we compared the algorithms in terms of accuracy and speed.

The distributions of the identified γ value from 100 windowed signals are shown in Fig. 3 for three different windows, and the identified γ can also be found in Table I. For the shortest window of 3.2 ns, we observe a large standard deviation in the distribution of the γ values for the NFT-based methods, while many of the identified γ are on the edge of the grid. The SSFM-based method also shows a large standard deviation, but close to the expected value of $\gamma = 1.20$ 1/(W·km) identified from the full bursts. This window is barely large enough to effectively identify the value of γ using the SSFM-based method, while both NFT-based methods contain too many outliers to be reliable. Upon inspection, it indeed turned out that there were only about 15 eigenvalues within this windowed signal type, of which only a few were high enough to be unaffected by the windowing.

The window of 5.6 ns duration shows clearly distinguishable peaks around the expected value for γ. For this window size, the SSFM-based method becomes reliable, and the fast NFT-based method with 10 eigenvalues is closer to the expected γ value than the full NFT. This is likely because the full NFT contains many low eigenvalues that become unreliable when the signal is windowed. Although the low eigenvalues have a limited influence on the error in 13a, they can still bias the estimate. The bias towards higher values of γ is again attributed to random good matchings that are more likely due to the denser cloud of eigenvalues at higher nonlinearities. Next, the 8 ns window shows clear peaks in all distributions, and the full NFT and refined NFT show similar distributions. However, both NFT-based estimates show a clear deviation from the SSFM-based method, and are about 5% higher. The windowing thus seems to structurally bias both NFT-based methods. We also investigated other intermediate window durations, but these results were very similar to the shown results (or simply interpolations) and were therefore omitted from this article.

Finally, we also investigated the influence of the considered number of high eigenvalues K^{high} for the fast NFT-based method on the identified γ. We compared $k^{\text{high}} \in \{5, 8, 10, 12, 15\}$, with the result shown in Fig. 4. Overall, the distributions of the identified γ depend marginally on the chosen K^{high}, although for $K^{\text{high}} = 15$ we found that the bias towards higher γ increases, probably due to considering several low eigenvalues that are influenced by the windowing of the signal. While considering only 5 eigenvalues may put too much weight on single good or bad matchings of eigenvalues, we find that considering between 5–10 eigenvalues leads to results closest to the correct γ. Nevertheless, the influence of K^{high} is still rather limited.

The computation times for the windowed signals are indicated in Table I. We observe that the computation time for the SSFM-based method scales approximately linearly with the number of signal samples. As expected, both NFT-based methods scale worse with the number of signal samples than the SSFM based method. Reducing the window to the minimum required length therefore in particular speeds up the NFT-based methods. However, we observed that this can cause a structural deviation in the identified γ value, or causes the methods to fail entirely due to a

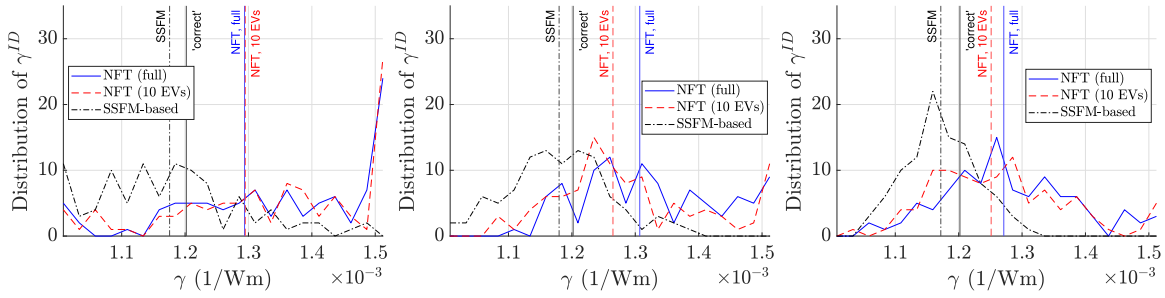

(a) 3.2 ns window (b) 5.6 ns window (c) 8.0 ns window

Fig. 3. Distributions of identified γ from a windowed raised-cosine signal for various window durations.

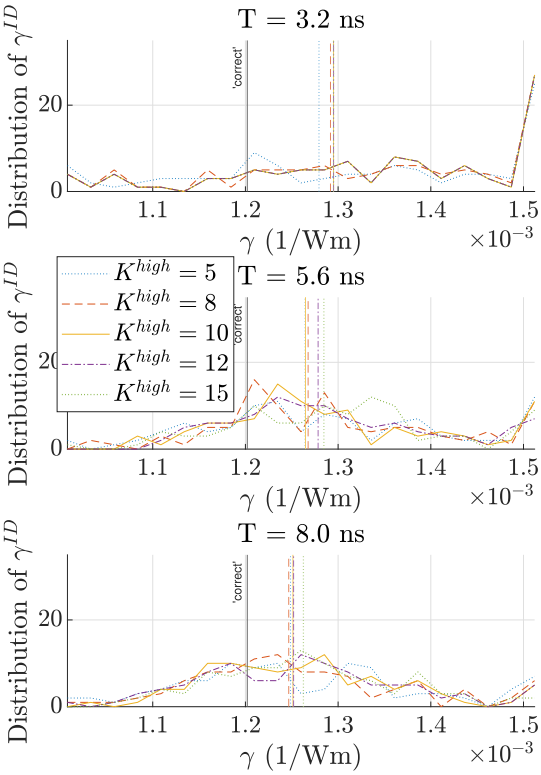

Fig. 4. Identified γ from windowed signals using a varying number of high eigenvalues K^{high}.

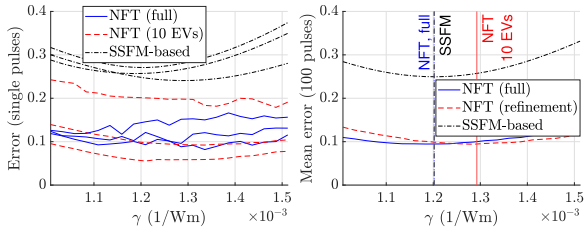

(a) Error from three different vanishing pulses. (b) The error, averaged over 100 vanishing pulses.

Fig. 5. Error-curves of the SSFM-based method and the NFT-based methods for the raised cosine pulse with vanishing tails, from Section V-B and Fig. 2.

lack of high eigenvalues. Furthermore, the NFT-based methods required 180 samples before the distribution for the identified γ value stabilized, and at this point the SSFM-based method is already faster. We thus conclude that the SSFM-based method yields more accurate and faster results than both NFT-based methods for the considered 1600 km SSFM link.

D. Discussion

In this section, we discuss several possible improvements to SSFM- and NFT-based identification methods, and share our view on the feasibility for each option.

Accuracy and consistency: In the shown examples, the SSFM-based method consistently identified $\gamma \approx 1.20$ 1/(W·km), whereas the NFT-based estimates were often biased, as well as that the estimates had a larger standard deviation. In particular the bias of up to 7% for the NFT-based methods can be too large to be acceptable in some cases. To investigate the reason for the larger standard deviation, the error-curves of the full bursts from Section V-B are shown in Fig. 5. When considering the average error in Fig. 5(b), we observe that the NFT- and SSFM-based errors show a clear optimum. However, we observe that for a single burst the SSFM-based method has a much smoother error-curve than the full NFT-based method. This is caused by sudden changes in the eigenvalue matching as γ is varied. The NFT-based method with only 10 eigenvalues is much smoother, as the high input- and output-eigenvalues usually stay matched in the same pairs, while the error only changes because the eigenvalues drift away/closer as γ is varied. However, as discussed before, the NFT-based matching using only high eigenvalues seems to be biased towards high γ values. We note here that the NFT-based method could be biased as it is optimizing a different criterion: it attempts to only match the eigenvalues as well as possible, instead of the full signals. It may therefore be possible that the NFT-based γ value is optimal in this sense. However, our observations suggest that this is not the case. We believe the bias is introduced due to the denser clouds of eigenvalues at higher γ values that allow for random good matchings. While it might be possible to account for this effect, it seems challenging to do so.

Computation time: We observed that the NFT-based methods can be faster than the SSFM-based method when the fiber length is long and the signal is short, but for the 1600 km link the SSFM-based method is usually faster. However, both the

NFT-based methods and SSFM-based methods can be further sped up in various ways. For the NFT-based methods, the most important constraint is the calculation of the discrete spectrum, which takes $\mathcal{O}(N^2)$ FLOPs for the method used in this article, which may also be observed in Table I. When comparing the computation time per signal as a function of the number of signal samples, we indeed observe this relation for the full NFT-based method. The fast NFT-based method uses only two full NFTs for the first grid point, but the refinement-based NFTs for all other grid points require only $\mathcal{O}(N)$ time, so the $\mathcal{O}(N^2)$ scaling is much less visible there. Especially signals with large bandwidths will require more samples to capture, and thus take longer computation times for NFT-based methods (see e.g. the 42 GB scenario). This drawback would pose a problem as the current trend in optical communication is towards high data rates, which are associated with large bandwidths.

Fortunately, recent research has shown that the higher eigenvalues of a signal may be determined quickly using both time windowing *and* frequency windowing [31]. While we were already using some form of time-windowing in this article, the paper [31] showed that frequency windowing (i.e., partitioning the full signal into band-limited signals, calculating the eigenvalues of each frequency-windowed partition, and then recombining the discrete spectra) could drastically reduce the computation time for calculating the higher eigenvalues from signals with large bandwidth. This would largely overcome the drawback of computational scaling in the signal bandwidth associated with NFT-based identification methods. In scenarios with higher bandwidths than in our experiments, an additional frequency windowing step as in [31] is thus recommended to reduce computation times.

The SSFM-based method could be sped up further, for example by using Volterra series for the digital propagation (see e.g., [32]), which require less steps per span for similar accuracy. Furthermore, due to the observed smoothness in the error-curves for the SSFM-based method, the grid search could be replaced by a local-descend method, allowing for even faster identification. We shortly investigated this possibility, and found that the SSFM-based error already converged in approximately four steps to the optimal γ value using Newton's method due to its smooth error-curves.

Dependence on power spectral density: In order to identify the nonlinearity coefficient, the signal needs to have a sufficiently high power spectral density such that the nonlinear effects become observable. We shortly consider two cases here with lower power spectral density, and compare how the identification methods perform. The results are shown in Fig. 6. The left case considers the same windowed raised cosine signal as from Fig. 3(c), but with only -4 dBm launch power (four times lower). The right case considers a raised cosine signal at 2 dBm launch power, but with symbol time T four times shorter. This also increases the bandwidth by a factor four, and hence the power spectral density is also four times lower. We observe that the SSFM-based method can still yield reliable estimates, whereas the NFT-based method fails entirely in most of the cases. For smaller power spectral densities, there are much fewer high eigenvalues. As a result the NFT-based methods become very biased towards higher γ values, for which there are more eigenvalues to be matched. We thus observe that the SSFM-based method is also more robust for identification on signals with low power spectral densities. We note here that for low-power signals, the continuous spectrum contains a larger portion of the signal energy and might be used to identify γ.

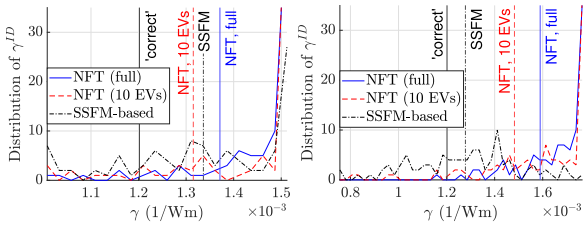

(a) 8 ns, 13 GHz, -4 dBm (b) 11 ns, 42 GHz, 2 dBm

Fig. 6. Identified γ values for two signal types (duration, bandwidth and power as indicated) where the NFT-based method fails. The left signal type was a raised cosine with too little power for high eigenvalues. The right signal had a broader spectrum, with the same power, and therefore less power per Hz, also resulting in too low eigenvalues. As a result, most of the NFT-based estimates do not converge within the grid. However, the SSFM-based method still shows a peak near the expected value for the right case.

VI. Simulation Results for Links up to 8000 km, With Ideal Raman Amplification

In this section, we investigate a scenario in which NFT-based identification should outperform the SSFM-based identification. We will consider simulation data of an 8000 km fiber link, with ideal Raman amplification to ensure a uniform signal energy profile throughout the propagation. This scenario with long link lengths and ideal Raman amplification should be especially suitable for NFT-based identification, as the path-average approximation (8) is no longer required due to the ideal Raman amplification. Furthermore, the computation time of the SSFM-based method will be about 5 times as long as compared to the 1600 km link due to the increased link length, whereas the NFT-based methods are not directly influenced. Due to practical limitations, we were not able to demonstrate this example experimentally, and we present here results from simulated data instead. Finally, we estimate at which distance NFT-based methods are faster than the SSFM-based method, by also considering simulated links of 1600 km and 4800 km.

A. Simulation Channel

The considered link in the simulations had a total length of 8000 km, while the propagation was simulated with the NLSE from 1, with $\beta_2^{\text{ref}} = -21.2\frac{\text{fs}^2}{\text{km}}$ ($D = 16.6\frac{\text{ps}}{\text{nm·km}}$), $\gamma^{\text{ref}} = 1.20\,1/(\text{W·km})$, such that the simulated fiber corresponded to the experimental fiber. The loss parameter was set to $\alpha^{\text{ref}} = 0\frac{\text{dB}}{\text{km}}$ in the simulation due to the ideal Raman amplification. The propagation was performed by a split-step method, with steps of 2 km. At the end of every step, realistic Raman noise was added to the signal, with spontaneous emission factor of $n_{sp} = 3.5$, corresponding to a pump wavelength at approximately 1450 nm and a carrier wavelength of 1550 nm [33, Eq. 7.3.9].

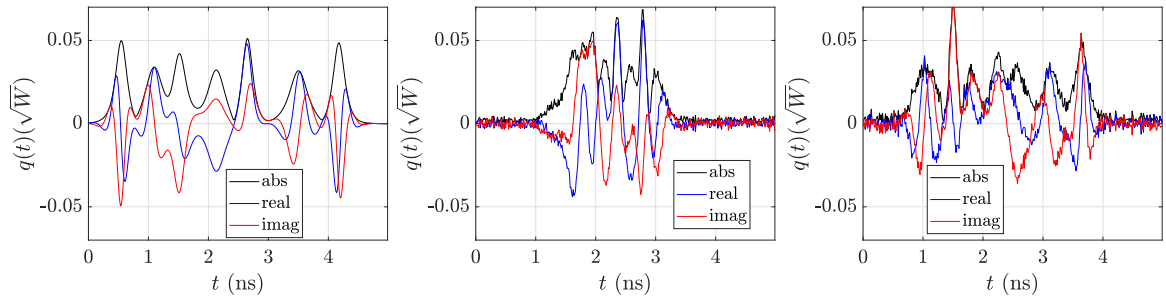

(a) 7-eigenvalue signal, $z = 0$ km. (b) 7-eigenvalue signal, $z = 4000$ km. (c) 7-eigenvalue signal, $z = 8000$ km.

Fig. 7. Example of a realization of a 7-eigenvalue signal traveling through an ideally Raman amplified single mode fiber of 8000 km length, at transmitter ($z = 0$), halfway ($z = 4000$ km), and at the receiver ($z = 8000$ km).

B. Signal Types

For the simulation, we considered two types of signals: a raised cosine-signal, similar to the one in the previous section, and a 7-eigenvalue signal, tailored to the fiber and designed to mitigate signal broadening, inspired by [34].

First, we considered a 7-eigenvalue signal. The signal was generated by initializing the NFT spectrum with 7 eigenvalues in the discrete spectrum, and $b(\lambda) = 0, \forall \lambda \in \mathbb{R}$ for the continuous spectrum. In a normalized domain (using $c_q = 2.38 \cdot 10^{11}$ 1/(s $\sqrt{\text{W}}$), $T_0 = 1$ s and 10), we set the eigenvalues as $\lambda = 10^9[-7.5 + 5.7i, -5.0 + 3.8i, -2.5 + 5.7i, 0 + 3.8i, 2.5 + 5.7i, 5.0 + 3.8i, 7.5 + 5.6i]$, respectively with absolute b-coefficients $\log|b| = [-18.7, -9.12, -10.38, -2.62, 1.14, 6.24, 15.86]$. The phases of the b-coefficients were randomly assigned to $\pm\pi/4$ or $\pm 3\pi/4$. The bandwidth of this type of signal was approximately 9 GHz. This type of signal corresponds to eigenvalue communication, in which the bits are modulated with QPSK on the phase of the b-coefficient of each eigenvalue. The signal was designed such that the left-most soliton travels to the right and vice versa during the propagation over 8000 km. The effective duration of the signal thus first gets shorter, before getting wider again, and reaching the receiver at the approximate same duration as the transmitted signal. This type of eigenvalue communication signal is illustrated in Fig. 7. The launch power of this signal was -3.7 dBm.

Second, we considered the same raised-cosine signal as in the previous section with $N_c = 128$ symbols per block, and $T^c = 0.1$ ns, but adding an 11.2 ns guard interval (instead of 3.2 ns), resulting in blocks of 24 ns. The additional guard interval is required to prevent interference between two blocks, as the additional link length causes each block to spread out much further. We set the average launch power to -4 dBm. This launch power with Raman amplification roughly leads to the same path-average power as +2 dBm launch power for the previous link with lumped amplification. The exact same transmitted 7-eigenvalue signals and raised cosine signals were also used for propagation over 1600 km and 4800 km. We note here that the long guard intervals required for the 8000 km transmission were excessive for the 1600 km and 4800 km transmission, but we chose to still include the long guard intervals to make the comparison fair.

C. Identification From Simulated Signals

We identified γ from both mentioned types of signals, using both NFT-based methods, and the SSFM-based method. First we considered the full blocks of the 7-eigenvalue type signals, second the full blocks of the raised-cosine type signals, and third the windowed raised-cosine type signals, where each window contained only the middle 50% of each block.

The identified γ value for each signal type, each method and each fiber length are shown in Table I. As the γ distributions were very similar for the three considered link lengths, we only show the result for 8000 km in Fig. 8. We observe that for the 7-eigenvalue type signal, all three methods yield very accurate results, although the fast NFT-based method shows a slightly larger variance in the identified γ than the other two methods. For both the full and the 50% windows of the raised cosine-type signals, the full NFT-based method as well as the SSFM-based methods again yield highly accurate results with low variance, but the fast NFT-based method again shows a small bias towards higher γ values, and has larger variance. In all scenarios the SSFM-based method yields accurate results with the lowest variance, and is therefore the most accurate method.

However, when comparing the computation times in Table I for the 8000 km link, we observe that the full NFT-based method is significantly faster than the SSFM-based method except for the longest signal, and the fast NFT-based method is consistently 4 times as fast as the SSFM-based method for all types of signals. We thus conclude that the NFT-based methods can indeed provide a significant speed up for very long links, at the cost of a small loss in accuracy and increase in uncertainty. Fig. 9 also shows that the full NFT-based method is faster than the SSFM-based method for the 7-eigenvalue (7-EV) signal already at 2000 km, and for the other two signals comparably fast at 8000 km. The fast NFT-based method using only the 10 highest eigenvalues is already faster for all considered signals for links longer than 2000 km, and much faster at 8000 km.

VII. Conclusion

We compared three different methods for identifying the Kerr-nonlinearity coefficient for an installed optical single-mode fiber link from available transmission data. The first method was

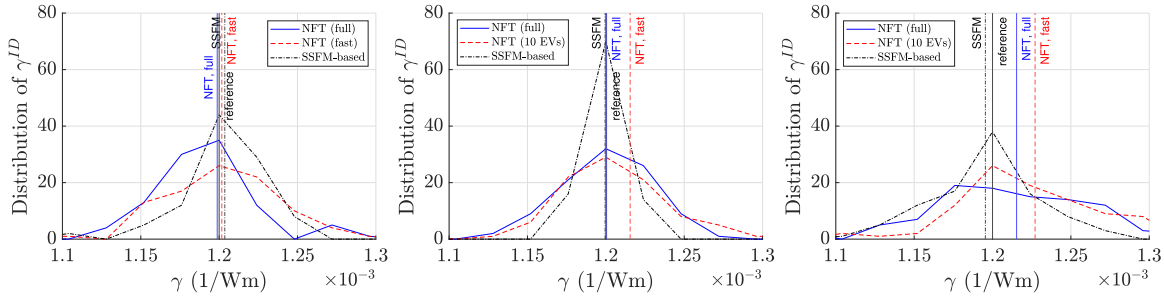

(a) 7-eigenvalue type signal, full block (b) Raised-cosine type signal, full block (c) Raised-cosine type signal, half block

Fig. 8. Identified γ for the SSFM with ideal Raman amplification from 8000 km transmission data. The distributions for 4800 km and 1600 km were similar, and are therefore omitted.

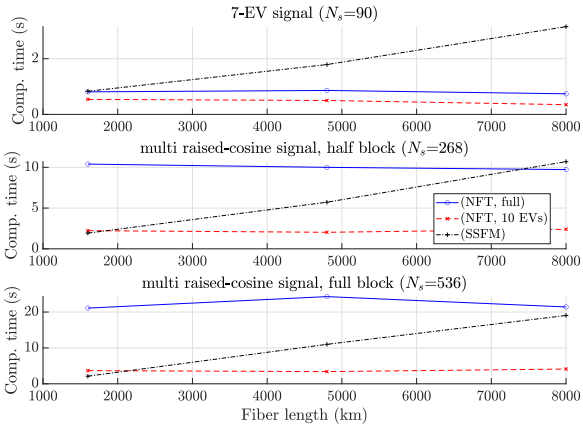

Fig. 9. The mean computation time per signal for each simulated signal as a function of fiber length, also shown in Table I). The computation times for the NFT-based methods remain approximately constant, whereas the SSFM-based method increases linearly with distance.

based on numerical split-step propagation of the transmitted signal and comparing input and output. The second method compared all solitonic eigenvalues at input and output using the nonlinear Fourier transform (NFT). The third method only compared the highest few eigenvalues, and calculated these faster using local refinement of previous eigenvalues. The third method was first proposed in this article. We compared these three methods on complete bursts, and on cut-out parts of bursts, for which we adapted the SSFM-based method to deal with interference due to the channel memory.

We showed that the SSFM-based method was faster and more accurate than both NFT-based identification methods for an experimental 1600 km link. The NFT-based method with few eigenvalues was significantly faster than the full NFT-based method, but showed some bias when compared using complete bursts with vanishing tails. When applied on a windowed signal without vanishing tails, both NFT-based methods showed some bias, but the method with few eigenvalues was more accurate in this case. Nevertheless, the SSFM-based method was more accurate in all aspects for both the vanishing pulse, and the windowed signal. We thus consider the SSFM-based method to be the method of choice for the identification of the nonlinearity coefficient in operational single-mode fibers at equivalent transmission distances.

Finally, we investigated whether NFT-based identification could outperform SSFM-based identification for a very long link of 8000 km. Indeed the NFT-based methods did not scale with the link length, and showed similar or lower computation times than the SSFM-based method when applied to signals for a simulated ideal-Raman amplified link, although the SSFM-based method was still slightly more accurate. In case that a small loss in accuracy is acceptable, the NFT-based method could therefore be the method of choice for long links.

REFERENCES

[1] G. P. Agrawal, *Fiber-Optic Communication Systems*, vol. 222. Hoboken, NJ, USA: Wiley, 2012.
[2] M. Secondini, D. Marsella, and E. Forestieri, "Enhanced split-step Fourier method for digital backpropagation," in *Proc. IEEE Eur. Conf. Opt. Commun.*, 2014, pp. 1–3.
[3] R. Dar and P. J. Winzer, "Nonlinear interference mitigation: Methods and potential gain," *J. Lightw. Technol.*, vol. 35, no. 4, pp. 903–930, Feb. 2017.
[4] E. Ip and J. M. Kahn, "Compensation of dispersion and nonlinear impairments using digital backpropagation," *J. Lightw. Technol.*, vol. 26, no. 20, pp. 3416–3425, Oct. 2008.
[5] S. K. Turitsyn et al., "Nonlinear Fourier transform for optical data processing and transmission: Advances and perspectives," *Optica*, vol. 4, no. 3, pp. 307–322, 2017.
[6] R.-J. Essiambre, G. Kramer, P. J. Winzer, G. J. Foschini, and B. Goebel, "Capacity limits of optical fiber networks," *J. Lightw. Technol.*, vol. 28, no. 4, pp. 662–701, Feb. 2010.
[7] P. André and J. Pinto, "Simultaneous measurement of the nonlinear refractive index and chromatic dispersion of optical fibers by four-wave mixing," *Microw. Opt. Technol. Lett.*, vol. 34, no. 4, pp. 305–307, 2002.
[8] T. Kato, Y. Suetsugu, M. Takagi, E. Sasaoka, and M. Nishimura, "Measurement of the nonlinear refractive index in optical fiber by the cross-phase-modulation method with depolarized pump light," *Opt. Lett.*, vol. 20, no. 9, pp. 988–990, 1995.
[9] A. Boskovic, S. Chernikov, J. Taylor, L. Gruner-Nielsen, and O. Levring, "Direct continuous-wave measurement of n_2 in various types of telecommunication fiber at 1.55 μm," *Opt. Lett.*, vol. 21, no. 24, pp. 1966–1968, 1996.
[10] C.-Y. Lin et al., "Adaptive digital back-propagation for optical communication systems," in *Proc. IEEE Opt. Fiber Commun. Conf.*, 2014, pp. 1–3.
[11] M. Piels, E. P. da Silva, D. Zibar, and R. Borkowski, "Performance emulation and parameter estimation for nonlinear fibre-optic links," in *Proc. IEEE 21st Eur. Conf. Netw. Opt. Commun.*, 2016, pp. 1–5.
[12] L. Jiang et al., "Chromatic dispersion, nonlinear parameter, and modulation Format monitoring based on Godard's error for coherent optical transmission systems," *IEEE Photon. J.*, vol. 10, no. 1, pp. 1–12, Feb. 2018.

[13] J. K. Andersen et al., "Path average measurements of optical fiber nonlinearity using solitons," *J. Lightw. Technol.*, vol. 16, no. 12, pp. 2328–2335, Dec. 1998.
[14] P. de Koster and S. Wahls, "Dispersion and nonlinearity identification for single-mode fibers using the nonlinear Fourier transform," *J. Lightw. Technol.*, vol. 38, no. 12, pp. 3252–3260, Jun. 2020.
[15] P. de Koster, J. Koch, O. Schulz, S. Pachnicke, and S. Wahls, "Experimental validation of nonlinear Fourier transform-based kerr-nonlinearity identification over a 1600 km SSMF link," in *Proc. IEEE Opt. Fiber Commun. Conf.*, 2022, pp. 1–3.
[16] S. Turitsyn, E. Sedov, A. Redyuk, and M. Fedoruk, "Nonlinear spectrum of conventional OFDM and WDM return-to-zero signals in nonlinear channel," *J. Lightw. Technol.*, vol. 38, no. 2, pp. 352–358, Jan. 2020.
[17] P. de Koster, J. Koch, S. Pachnicke, and S. Wahls, "Experimental investigation of nonlinear Fourier transform based fibre nonlinearity characterisation," in *Proc. IEEE Eur. Conf. Opt. Commun.*, 2021, pp. 1–4.
[18] G. Agrawal, " *Nonlinear Fiber Optics*, 5th ed. Amsterdam, The Netherlands: Elsevier, 2010.
[19] R. Pleban, A. Azari, R. Salem, and T. E. Murphy, "SSPROP." Accessed: May 31, 2022. [Online]. Available: https://photonics.umd.edu/software/ssprop/
[20] S. Wahls, S. T. Le, J. E. Prilepsk, H. V. Poor, and S. K. Turitsyn, "Digital backpropagation in the nonlinear Fourier domain," in *Proc. IEEE 16th Int. Workshop Signal Process. Adv. Wireless Commun.*, 2015, pp. 445–449.
[21] M. I. Yousefi and F. R. Kschischang, "Information transmission using the nonlinear Fourier transform, part I: Mathematical tools," *IEEE Trans. Inf. Theory*, vol. 60, no. 7, pp. 4312–4328, Jul. 2014.
[22] A. Shabat and V. Zakharov, "Exact theory of two-dimensional self-focusing and one-dimensionalself-modulation of waves in nonlinear media," *Sov. Phys. JETP*, vol. 34, no. 1, pp. 62–69, 1972.
[23] M. J. Ablowitz, D. J. Kaup, A. C. Newell, and H. Segur, "The inverse scattering transform-fourier analysis for nonlinear problems," *Stud. Appl. Math.*, vol. 53, no. 4, pp. 249–315, 1974.
[24] S. Chimmalgi and S. Wahls, "Bounds on the transmit power of b-modulated NFDM systems in anomalous dispersion fiber," *Entropy*, vol. 22, no. 6, 2020, Art. no. 639.
[25] T. Gui, G. Zhou, C. Lu, A. P. T. Lau, and S. Wahls, "Nonlinear frequency division multiplexing with b-modulation: Shifting the energy barrier," *Opt. Exp.*, vol. 26, no. 21, pp. 27978–27990, 2018.
[26] H. W. Kuhn, "The hungarian method for the assignment problem," *Nav. Res. Logistics Quart.*, vol. 2, no. 1/2, pp. 83–97, 1955.
[27] S. Wahls, S. Chimmalgi, and P. Prins, "FNFT: A software library for computing nonlinear Fourier transforms," *J. Open Source Softw.*, vol. 3, p. 597, 2018, doi: 10.21105/joss.00597.
[28] S. Pachnicke, *Fiber-Optic Transmission Networks: Efficient Design and Dynamic Operation*. Berlin, Germany: Springer, 2011.
[29] P. Kabaciński, T. M. Kardaś, Y. Stepanenko, and C. Radzewicz, "Nonlinear refractive index measurement by SPM-induced phase regression," *Opt. Exp.*, vol. 27, no. 8, pp. 11018–11028, 2019.
[30] T. D. De Menezes et al., "Nonlinear spectrum modulation in the anomalous dispersion regime using second-and third-order solitons," *Photonics*, vol. 9, no. 10, 2022, Art. no. 748.
[31] P. de Koster and S. Wahls, "Fast and reliable detection of significant solitons in signals with large time-bandwidth products," *J. Lightw. Technol.*, vol. 41, no. 20, pp. 6586–6598, Oct. 2023.
[32] L. Liu et al., "Intrachannel nonlinearity compensation by inverse volterra series transfer function," *J. Lightw. Technol.*, vol. 30, no. 3, pp. 310–316, Feb. 2012.
[33] G. P. Agrawal, *Fiber-Optic Communication Systems*, 5th ed. Hoboken, NJ, USA: Wiley, 2021.
[34] H. Buelow, V. Aref, and W. Idler, "Transmission of waveforms determined by 7 eigenvalues with PSK-modulated spectral amplitudes," in *Proc. IEEE 42nd Eur. Conf. Opt. Commun.*, 2016, pp. 1–3.